FORMATION, EVOLUTION AND ESTIMATED RADIANCE OF SURFACE FOGS IN LOW AND MIDDLE LATITUDES ON MARS

A. Inada, **W.J. Markiewicz**, *Max-Planck-Institut für Aeronomie, Katlenburg-Lindau, Germany (inada@linmpi.mpg.de)*, **T. Mukai**, *Graduate School of Science and Technology, Kobe University, Nada, Japan*.

Introduction: The existence of fog near the Martian surface was discussed by Flassar and Goody (1976) and Hess (1976) in context of preparations for the Viking Orbiter 1 mission. Indeed fog was observed in the Memnonia region (15.0°S, 145.0°W) by the camera on Viking Orbiter 1 (Briggs *et al*., 1977). A bright feather in Kasei Valley imaged by Mars Orbiter Camera (MOC) on Mars Global Surveyor is also considered to be surface fog. However, detail analysis of fog images have not been performed yet. The study of surface fog is important as part of the study of water cycle in the Martian atmosphere and the exchange of water between the atmosphere and the surface.

The observations of the Martian satellite Phobos at night with the cameras of Viking Landers and Mars Pathfinder discovered that the optical depth increased at the time between 2:00 and sunrise (Pollack *et al*., 1977, Thomas *et al.*, 1999). Since the increase coincides with the time of the lowest diurnal temperature, Pollack *et al*. (1977) suggested that it is due to the formation of night fog. Furthermore, Viking Landers measurements show night time periods with constant temperature 1.6 m above the ground. This was considered to be due to night fog (Ryan and Sharman, 1981).

Colburn *et al*. (1989) calculated the altitude dependence of water vapor partial pressure above the Viking Lander 1 site with the assumptions that water vapor is vertically well mixed and the column density of water is 11 pr. μm. They found that water vapor is saturated above 25 km most of the time and in the near surface layer (below 400 m) during winter. Formation of fogs was studied with a boundary layer model by Savijarvi (1995). He assumed column density of water vapor of 16 pr. μm. He found that a thin fog can appear from 22:00 to 7:00 with the maximum altitude of only 40 m and the amount of water ice in the fog is 0.43 pr. μm.

Microphysical processes were first introduced to the Martian cloud model by Michelangeli *et al*. (1993) and improved by Colaprete and Toon (2000). This cloud model was adapted by Inada (2002) to study formation of near surface fogs. The model description is found in the following section.

From the observations by the spacecraft Phobos 2, it was pointed out that the mixing ratio of water vapor was 135 ppm at the altitude of 10-25 km, the clouds level, and it decreased to 3±2 ppm above 30 km (Rodin *et al*., 1997). More recently, from the data of the Imager for Mars Pathfinder (IMP) it was concluded that the water vapor was concentrated to 1-3 km near the surface and the mixing ratio might reach 600 ppm in this layer (Titov *et al*., 1999). Colaprete and Toon (2000) have also shown that after high altitude clouds form about 60 % of water vapor is located below a few kilometers above the surface. This is because the water ice coated cloud particles sediment to lower layers and water ice sublimates there. This non-uniform vertical water vapor distribution is taken into account in the present fog model.

The model predicts the time of fog occurrence, its vertical extent, size distribution of fog particles and amount of water ice within it. Furthermore, we present the predicted spectra of the fog in the optical and thermal wavelength range. It is shown that the observation in the thermal region is useful for detection of even thin fog.

Fog Model: The model includes the microphysical processes of nucleation, condensation and sublimation. Aerosols are transported vertically by sedimentation and turbulence. Martian atmosphere is loaded with dust particles. When water vapor partial pressure is above the point of saturation the water ice nucleates on the surface of the dust particles (heterogeneous nucleation) rather then in gas phase (homogeneous nucleation). This model follows the formulation of Michelangeli *et al.* (1993) and other authors mentioned above. Coagulation is not taken into account here for computational reasons. Brownian coagulation is only important for the very small particles which do not play a role in fog formation (see below). Coagulation due to sedimentation or turbulence has not been discussed to date in the Mars context.

The initial dust size distribution is assumed to be a modified gamma with effective radius, r_{eff} = 1.85 μm and effective variance, v_{eff} = 0.25, as derived from the IMP sky images (Markiewicz *et al.*, 1999). The aerosol size bins are set to increase logarithmically, and the number of the size bins is 41 ranging from 0.01 to 100 μm. The initial dust is distributed vertically with a constant mixing ratio with the scale height h = 12.5 km, and the optical depth τ = 0.61 at the wavelength λ = 896.1 nm.

In the model the atmosphere is divided into 25 vertical layers. The thickness of the *i*th layer, $dz_i=1.2^i dz_0$, where dz_0=25.0 m is the thickness of the lowest layer. This grid extends therefore to altitude of 11.8 km. The aerosols that precipitate to the

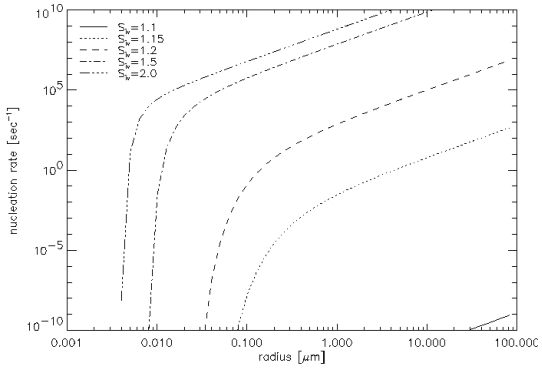

Fig. 1. The nucleation rates on a spherical particle verses its radius for several values of saturation S_{vi}. The temperature is 200 K and the wetting coefficient is 0.925.

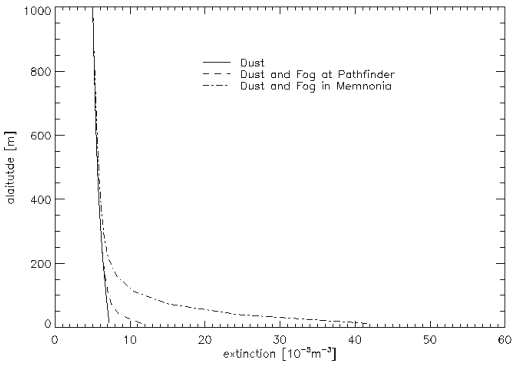

Fig. 3. Extinction of the atmosphere without fog (solid line), and with fogs at the Mars Pathfinder landing site (dashed line) and in the Memnonia region (dash-doted line).

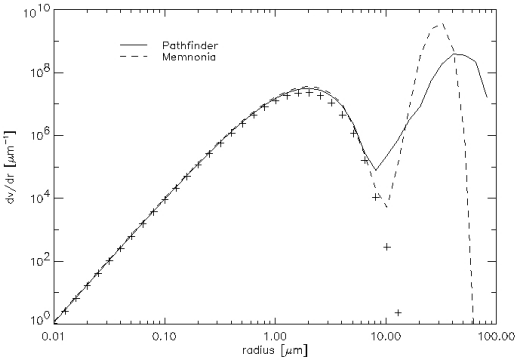

Fig. 2. Volume size distribution of aerosols at 7:00 LOC simulated at the Mars Pathfinder landing site (solid line) and in the Memnonia region (dashed line). Cross symbols show the initial dust distribution.

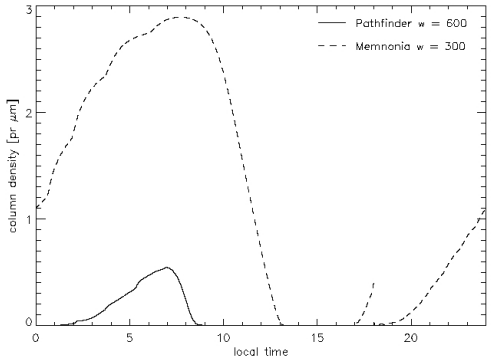

Fig. 4. Column density of water ice in fogs at the Mars Pathfinder landing site (solid line) and in the Memnonia region (dashed line). The simulations begin at 18:00.

lowest layer remain there until their ice shells sublimate enough for them to be transported upwards again. In reality some of this particles will settle down to the surface, the total number of these particles is however small as can be seen from Figure 3.

The vertical profiles of temperature and pressure are taken from the European Martian Climate Database (Forget *et al*., 1999). Since the formed fogs are thin, the effect of fog on these profiles is ignored. The simulations are performed for two cases. The first is the Mars Pathfinder landing site (19.2°N, 33.2°W) in late summer with the aerocentric longitude of the Sun, L_s = 150°. The mixing ratio of water vapor in the 3 km thick surface layer was derived from IMP data to be 600 ppm. The second simulation is for the Memnonia region in early winter (L_s = 99°), when fog was imaged there by Viking Orbiter 1. Since the Memnonia region is located higher than the Mars Pathfinder landing site and the amount of water vapor is generally smaller during winter, the mixing ratio of 300 ppm is assumed for this simulation. In both cases it is assumed that there is no water vapor above the altitude of 3 km to prevent cloud formation.

Nucleation Rate. Heterogeneous nucleation rate depends on the radius of substrate, the wetting coefficient, which is the cosine of the contact angle, and water vapor saturation (Purppacher and Kelett, 1978). Since the wetting coefficient of Martian dust is not known, it is assumed to be 0.975 following the value of the dust with pre-activation as used by Michelangeli *et al.* (1993). Figure 1 shows the nucleation rates for various saturation ratios S_{vi}, and temperature of 200 K chosen as a typical night condition near the surface. It shows that nucleation on small dust particles requires high saturation ratio. The nucleation rate increase, however, rapidly with the size of the dust particles. Hence, large particles will be coated with ice faster by nucleation alone. Since they also have larger surface area, the subsequent condensation on these particles will remove largest fraction of water vapor that is converted to ice. The saturation ratio does not increase significantly as the temperature decreases. Consequently, few small dust particles are covered by water ice and the rest remains as dust. The results below confirm that fog is produced on large dust particles only (*cf.* Figure 2).

Results of the Fog model. The simulations are started at 18:00 Martian local time and last for 1 day. The volume size distribution of aerosols at 7:00 in the 25 m thick layer above the surface is shown in

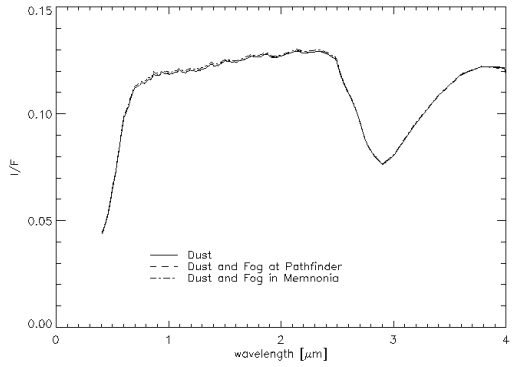

Fig. 5. Upward radiance scaled by incoming solar flux at the top of the atmosphere in the optical wavelength range. The cases shown are the same as Fig. 3.

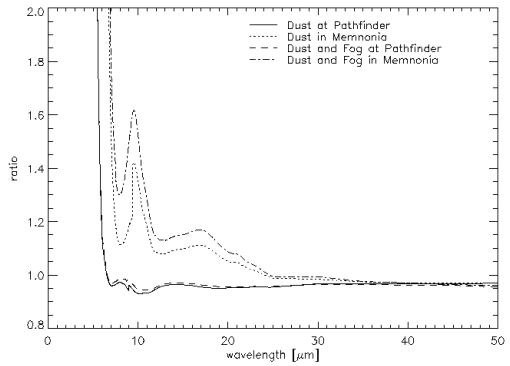

Fig. 6. Ratio of the upward thermal radiance at the top of the atmosphere to that of a blackbody with the temperature of the surface at 7:00 LOC for the two cases studied.

Figure 2 for both Mars Pathfinder landing site and Memnonis region. For reference the initial dust distribution is also shown. The 7 o'clock distribution is clearly bimodal with the particles with radius below several microns following the initial distribution. These particles have not changed in size and therefore have negligible amount of water ice on their surface. The particles above this threshold have significantly grown in size. The mean radius of this population is around 50 and 30 μm at the Mars Pathfinder landing site and in the Memnonia region respectively. The difference for these two places is due to the different values of the mixing ratio and temperature.

The extinction of atmosphere for both simulations is shown in Figure 3 with the reference to one with only dust particles. Thin fogs appear below the altitude of about 200 m. Since the temperature of atmosphere in the Memnonia region is lower than at the Mars Pathfinder landing site in these simulations, more water ice particles are formed above the Memnonia region. Figure 4 shows the diurnal variation for the column densities of water ice in fogs. At the Mars Pathfinder site the fog forms at midnight, becomes thickest in the early morning, and disappears at about 8:30. The maximum column density is 0.75 pr. μm. This is much smaller than the maximum of 2.9 pr. μm in the Memnonia region. The precipitated fog particles sublimate near the surface, hence it is seen that the water vapor is saturated earlier, at 17:00, before the next simulation day.

Radiative Transfer Model: We next consider the effect of fog on the radiance as it might be observed by an orbiter. The radiative transfer is calculated with the spherical harmonics discrete ordinate method (SHDOM) (Evans, 1998). Here one dimensional version of SHDOM is used. The calculation includes reflected light and thermal emission and covers the wavelength range λ = 0.4 to 50 μm. The solar flux at the top of the Martian atmosphere is calculated considering the distance between the sun and Mars at each L_s. The sun zenith angle, *i*, is fixed to be 70° in all cases. The zenith angle of emission, *e*, is set to be 0° corresponding to nadir observations. Models of dust and fog particles are taken from the simulations of the previous section with the local solar time being 7:00. Their optical properties are computed using the Mie theory assuming the dust and the ice shells to be spherical. The refractive index of dust is taken from Ockert-Bell *et al.* (1997) and extended to 50 μm (A. Rodin, private communication). The refractive index of water ice is taken from Warren (1984). Since water ice absorbs less in blue than the dust we expect the red/blue color ratio to be smaller for an atmosphere with fog than one without. The radiative transfer calculations show, however, that the fogs simulated here are too thin to have an effect on the radiance in the visible wavelength range (Figure 5). If the fog was much thicker, we would expect the water ice absorption band near λ=3 μm to be distinguishable from that for dust as is the case for atmosphere with water ice clouds. This is not the case here as can be seen in Figure 5. Furthermore the fog particles with large dust cores do not behave optically in the same way as pure water ice particles. The difference in radiance with and without fog is clearer in the thermal region where the surface emission is dominant (Figure 6). This figure shows the upward radiance at the top of the atmosphere normalized by that of the blackbody with the surface temperature corresponding to the fog model at 7:00. This temperature at the Mars Pathfinder landing site is 204.2 K and in the Memnonia region 165.4 K. The size parameter $x = 2\pi r/\lambda$, where r is radius of a particle, is much smaller for dust than for fog particles (*cf.* Figure 2). Hence fog particles are more forward scattering than the dust. This is particularly true in the approximate range 7 μm < λ < 25 μm, where *x* for fog particles is of order unity. Figure 6 shows that the fog at the Mars Pathfinder landing site is so thin and the surface temperature is so warm that the detection of the radiance from fog is difficult. The effect of the fog on radiance above the Memnonia region, however, is easily seen in this wavelength range.

Conclusions and Discussion: Our simulations

show that thin fogs appear in 200-m thick layer near the surface in both cases studied. The water ice in fogs reaches its maximum at 7:00 and 8:00 at the Mars Pathfinder Landing site and in the Memnonia region respectively. The temperature of the atmosphere in the Memnonia region is low enough for fog to be present until about midday. When fog is formed, the size distribution of aerosols is bimodal because only large dust particles act as seeds of the fog particles. The small dust is not covered by water ice since the ice nucleation rate decreases rapidly with particle size.

The radiance at the top of the atmosphere with fog is calculated as it might be measured by an orbiter instrument. It is shown that data in the wavelength range between 7 and 25 μm will be useful for detection of even thin fogs, which will not be detectable with nadir observations using visible or near infrared wavelength. In the thermal wavelength region, the nadir observation is efficient because fog particles have strong forward scattering.

Once fog is detected in the thermal wavelength, the size of large particles and the amount of water ice can be estimated by comparison with the model presented here. The fog formation depends on several parameters that are not well known: for example, the mixing ratio of water vapor near the surface, the wetting coefficient of dust, the vertical distribution of dust, exchange of water vapor between the atmosphere and the surface. The fog data will play a role to further constrain these parameters.

Acknowledgements: This research was carried out under the partial support of JSPS Postdoctoral Fellowships for Research Abroad.

References:

Briggs G. K. Klassen, T. Thorpe, J. Wellman and W. Baum, Martian Dynamical Phenomena During June-November 1976: Viking Orbiter Imaging Results, *J. Geophys. Res*., **82**, 4121-4149, 1977.

Colaprete A., O. B. Toon, and J. A. Magalhaes, Cloud formation under Mars Pathfinder conditions, *J. Geophys. Res*., **104**, 9043-9054, 1999.

Colaprete A., and O. B. Toon, The Radiative Effects of Martian Water Ice Clouds on the Local Atmospheric Temperature Profile, *Icarus*, **145**, 524-532, 2000.

Colburn, D. S., J. B. Pollack, and R. M. Haberle, Diurnal variations in optical depth at Mars, *Icarus*, **79**, 159-189, 1989.

Evans, K. F., The Spherical Harmonics Discrete Ordinate Method for Three-Dimensional Atmospheric Radiative Transfer, *J. Atmos. Scie.*, **55**, 429-446, 1998.

Flasar, F. M., and R. M. Goody, Diurnal behaviour of water on Mars, *Planet. Space Sci.*, **24**, 161-181, 1976.

Forget F., F. Hourdin, R. Fournier, C. Houdrin, O. Talagrand, M. Collins, S R. Lewis, P. L. Read, and J. Huot, Improved general circulation models of the Martian atmosphere from the surface to avove 80 km, *J. Geophys. Res*., **104**, 24155-24175, 1999.

Hess, S. L., The vertical distribution of water vapor in the atmosphere of Mars, *Icarus,* **28**, 269-278, 1976.

Inada A., Numerical Simulations of Martian Fog Formation and Inflight Calibration of Mars Imaging Camera on NOZOMI for its Future Observations, *Doctor thesis*, Kobe Univ., Kobe, 2002.

Markiewicz, W. J., R. M. Sablotny, H. U. Keller, N. Thomas, D. Titov, and P. H. Smith, Optical properties of the Martian aerosols as derived from Imager for Mars Pathfinder midday sky brightness data, *J. Geophys. Res*., **104**, 9009-9018, 1999.

Michelangeli, D. V.; O. B. Toon, R. M. Haberle, and J. B. Pollack, Numerical simulations of the formation and evolution of water ice clouds in the Martian atmosphere, *Icarus*, **102**, 261-285, 1993.

Pollack, J. B.; D. Colburn, R. Kahn, J. Hunter, W. van Camp, C. E. Carlston, and M. R. Wolf, Properties of aerosols in the Martian atmosphere, as inferred from Viking Lander imaging data, *J. Geophys. Res.,* **82**, 4479-4496, 1977.

Pruppacher, H. R, and J. D. Klett, *Microphysics of Clouds and Precipitation*, D. Reidel, Norwell, mass., 1978

Rodin A. V., O. I. Korablev, and V. I. Moroz, Vertical Distribution of Water in the Near-Equatorial Troposphere of Mars: Water Vapor and Clouds, *Icarus*, **125**, 212-229, 1997.

Ryan, J. A., and R. D. Sharman, H2O frost point detection on Mars, *J. Geophys. Res*., **86**, 503-511, 1981.

Savijarvi, H., A model study of the PBL structure on Mars and the earth, *Beitraege zur Physik der Atmosphaere* , **64**, 219-229, 1991.

Thomas, N., D. T. Britt, K. E Herkenhoff, S. L. Murchie, B. Semenov, H. U. Keller, and P. H. Smith, Observations of Phobos, Deimos, and bright stars with the Imager for Mars Pathfinder, *J. Geophys. Res*., **104**, 9055-9068, 1999.

Titov, D. V. W. J. Markiewicz, N. Thomas, H. U. Keller, R. M. Sablotny, M. G. Tomasko, M. T. Lemmon, and P. H. Smith, Measurements of the atmospheric water vapor on Mars by the Imager for Mars Pathfinder *J. Geophys. Res*., **104**, 9019-9026, 1999.

Toon, O. B., R. P. Turco, D. Westphal, R. Malone, and M. S. Liu, A multidimensional model for aerosols - Description of computational analogs, *J. Atmos. Sci.* , **45**, 2123-2143, 1988.

Warren, S. G., Optical constants of ice from the ultraviolet to the microwave, *Applied Optics*, **23**, 1206-1225, 1984.